



Porphyrin Organic Framework Hollow Spheres and Their Applications in Lithium–Sulfur Batteries

Bo-Quan Li, Shu-Yuan Zhang, Long Kong, Hong-Jie Peng, and Qiang Zhang*

Organic frameworks represent an emerging family of advanced materials that can be precisely controlled at the atomic level. However, morphology control of organic frameworks remains perplexing and difficult, strongly limiting the advantages of organic frameworks in multiple practical applications. Herein, porphyrin organic framework hollow spheres (POF-HSs) are fabricated by a template method as a proof of concept of organic frameworks with precisely controlled morphology. POF-HS exhibits explicit chemical structures of 2D POF and an expected hollow structure. The morphology of POF-HS is further regulated in terms of void size and shell thickness. Benefited from the polar chemical structures and the hollow spherical morphology, POF-HS sufficiently mitigates the shuttle of polysulfides by taking the dual effects of chemical adsorption and physical confinement and functions as a desirable host material for sulfur cathode to endow lithium–sulfur batteries with high capacity, long cycling life, and excellent rate performance. The accurate synthesis of POF-HSs demonstrates the highly controllable and versatile morphology of organic framework materials beyond precise integration of organic building blocks and represents infinite possibility of offering exotic organic frameworks for chemistry, sustainable energy, and material science.

Organic frameworks represent an emerging family of advanced materials that can be precisely controlled at the atomic level.^[1] Directed by reticular chemistry, organic building blocks with multifunctional groups are covalently linked into extended periodic skeletons, perfectly replicating the predesigned structures both chemically and geometrically.^[2] Since the first report by Yaghi and co-workers,^[3] organic frameworks demonstrate versatile applications in catalysis,^[4] gas storage,^[5] optoelectronics,^[6] molecular separation,^[7] and energy storage,^[8] and therefore have attracted extensive attention worldwide.

Despite the well-defined chemical structure, morphology control of organic frameworks remains perplexing and difficult. The interactions of organic framework microcrystallites are commonly noncovalent and weak, rendering random

stacking of the microcrystallites and disordered macrostructures thus far.^[9] Such disorderliness inevitably affords diversiform morphology of organic frameworks at macroscale, including belts,^[6] sheets,^[10] fibers,^[11] and cubes.^[12] The miscellaneous morphology renders intractable issues, for instance, heterogeneous contents, complicated interfaces, reduced surface area, and poor stability of organic frameworks, which are undesirable for practical applications. Therefore, accurate morphology control of organic frameworks is essential for full demonstration of their advantages and may bring extra benefits from a topotactic perspective.

Hollow sphere (HS) is regarded as a desirable morphology in many cases.^[13] Hollow spheres afford low density, large surface area for active sites' exposure, and improved structural stability. In addition, the inner hollow space allows the accommodation of guest contents to further realize specific functions.^[14] For instance,

Zhao et al. reported hollow MXene spheres for electrochemical sodium-ion storage,^[15] Sun and co-workers synthesized hollow iron–vanadium composite spheres as water oxidation electrocatalysts,^[16] and many other hollow structured materials have widely been applied in supercapacitors/batteries,^[17] electrocatalysis,^[18] and drug delivery.^[19]

Focused on organic frameworks, several pioneer works have reported a self-templated fabrication of hollow spherical organic frameworks by chemically adjusting the building blocks. Zhou et al. designed a 3D triptycene scaffold to suppress the interactions between monolayers, which further evolves into hollow spheres.^[20] Banerjee and co-workers synthesized the hollow spheres based on an inside-out Ostwald ripening process.^[21] Further researches indicate the planarity of building blocks and stacking efficiency contribute to the formation of hollow spherical structures.^[22] However, the self-templated method requires sophisticated organic building blocks and comprehensive synthetic procedures, of which both limit the implementation in other generalized systems. Besides, the morphology of these self-templated hollow spheres remains miscellaneous, implying the inefficiency for controllable synthesis of organic frameworks.

Template synthesis of organic frameworks offers a more universal and controllable pathway over the self-templated method by contrast. Abundant hollow structures are fabricated by introducing compatible templates as a pre-existing guide that

B.-Q. Li, S.-Y. Zhang, Dr. L. Kong, H.-J. Peng, Prof. Q. Zhang
Beijing Key Laboratory of Green Chemical Reaction Engineering
and Technology
Department of Chemical Engineering
Tsinghua University
Beijing 100084, China
E-mail: zhang-qiang@mails.tsinghua.edu.cn

The ORCID identification number(s) for the author(s) of this article can be found under <https://doi.org/10.1002/adma.201707483>.

DOI: 10.1002/adma.201707483

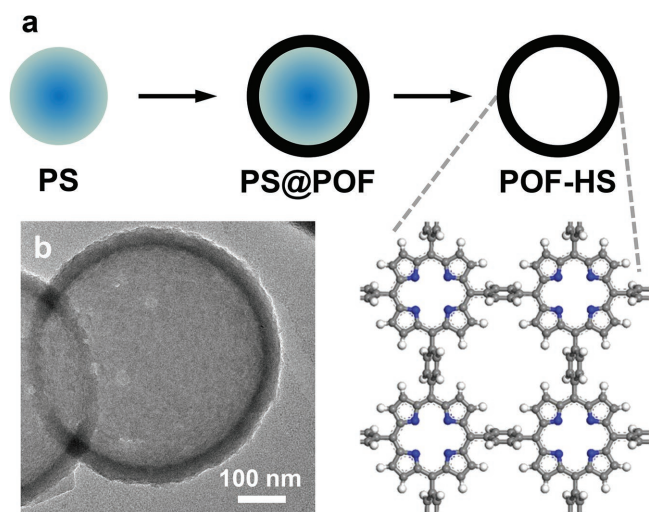


Figure 1. The concept of hollow spherical organic frameworks. a) Schematic for the synthesis of POF-HSs. The amplified image is the periodic structure of single-layer POF. b) TEM image of POF-HS with the typical hollow spherical morphology.

allows the morphology replicating of the given templates.^[23] For instance, hollow microporous organic networks served as templates for fabrication of hollow Co_3O_4 ,^[24] and Fe_3O_4 hollow spheres were synthesized using a quasiemulsion-templated method.^[25] Organic frameworks are also proved to be compatible with specific templates,^[26] and it is thereby highly expected to replicate organic framework hollow spheres from these properly chosen templates.

Herein, porphyrin organic framework hollow spheres (POF-HSs) are fabricated using polystyrene (PS) microspheres as the template. PS microsphere is a widely used template that can be easily manufactured and removed.^[27] POF, on the other hand, is selected because of its well-defined structure, simple synthetic methodology, and versatile functions. The as-synthesized POF-HSs exhibit an explicit hollow spherical morphology as well as identical chemical structure of POF. Both the void size and shell thickness of POF-HSs are easily regulated to afford various spherical hollow structures. By virtue of the polar chemical structures and the hollow spherical morphology, POF-HS is demonstrated as a favorable cathode host material in lithium–sulfur (Li–S) battery applications as it contributes to high capacity, long cycling life, and superior rate performance.

The synthetic routine of POF-HS is demonstrated in **Figure 1a**. PS microspheres with a diameter of 500 nm were selected as a proof-of-concept template to fabricate POF-HS with moderate size and shell thickness (Figure S1, Supporting Information). Typical synthesis of POF-HS involves an acid-catalyzed nucleophilic addition of stoichiometric benzene-1,4-dicarboxaldehyde and pyrrole to construct the porphyrin skeleton on PS leading to the formation of PS@POF, and subsequent removal of the PS templates by toluene treatment resulting in the targeted POF-HS. POF solid spheres (POF-SSs) were fabricated under otherwise identical conditions without PS template as the control sample.

Fourier-transformed infrared spectrometry was carried out to evaluate the completeness of the fabrication of POF-HS. As

demonstrated in Figure S2a in the Supporting Information, the carboxyl adsorption band at 1700 cm^{-1} is obviously reduced, indicating full conversion of the precursors into POF by dehydration. Other adsorption bands at lower wavenumbers are assigned to the stretching vibration and backbone deformation as intrinsic signals of POF.^[28] No characteristic adsorption band of PS was observed, implying the PS templates are completely removed (Figure S2b, Supporting Information). The structure of the resultant POF was elucidated by X-ray diffraction. Both POF-SS and POF-HS afford intense diffraction peaks at 13° (Figure S3, Supporting Information). The diffraction peaks manifest the intrinsic ordered structure of POF distinguished from amorphous polymers.

Transmission electron microscopy (TEM) image of POF-HS exhibits a hollow spherical contrast with bright inner space and dark outer shell (Figure 1b and Figure S4a, Supporting Information). The inner diameter and the thickness of POF-HS are estimated to be 500 and 40 nm, respectively, in agreement with the size of PS templates. The POF spheres are intact, discrete, and monodisperse (Figure S4b, Supporting Information). The high-resolution TEM image demonstrates a sheet morphology at the edge (Figure S4c, Supporting Information). The exotic 2D morphology is attributed to the intrinsic layered structure of POF-HS herein. Without the guidance of PS template, POF stacks into dense and solid spheres proved by the homogeneous contrast in the TEM image of POF-SS (Figure S5a, Supporting Information). POF-SS is uneven in size and rough at the edge with a diameter range of 1.0–3.0 μm (Figure S5b, Supporting Information). However, POF-SS exhibits similar sheet morphology as POF-HS at the edge, implying the shared microstructure of layered POF (Figure S5c, Supporting Information).

Element analysis was performed using X-ray photoelectron spectroscopy (XPS) and energy-disperse X-ray spectrometer (EDS). POF-HS exhibits an evident N content of 8.4 at.% and 9.7 at.% determined by XPS and EDS, respectively (**Figure 2a** and Figure S6a, Supporting Information). High-resolution N 1s XPS spectrum of POF-HS demonstrates pyrrolic N at 400.1 eV as the dominant N species with a fraction of 91.9% (Figure 2a, inserted). Other N species (refer to pyridinic N at 398.5 eV, quaternary N at 401.2 eV, and absorbed N at 405.6 eV) are negligible.^[29] The dominant pyrrolic N content is reasonable considering the pyrrole substrate and indicates the organic functional groups remained stable during synthesis. Further element mapping in Figure 2b demonstrates not only the uniform distribution of C and N but also the hollow morphology of POF-HS. The element contents of POF-SS are similar to POF-HS because of the same building blocks (Figures S6b and S7, Supporting Information).

The specific surface area of POF-HS is $304\text{ m}^2\text{ g}^{-1}$ using the multipoint Brunauer–Emmett–Teller method and approximates to that of $303\text{ m}^2\text{ g}^{-1}$ of POF-SS (Figure 2c). However, the nitrogen isotherm of POF-HS exhibits a significant rise at a high relative pressure, suggesting the macropore structure derived from the hollow interior. The quenched solid density function theory model was employed to analyze the pore structure. Compared with POF-SS, POF-HS exhibits a pore size distribution similar at the range from 1 to 10 nm but very different over 10 nm, featuring more abundant mesopores and macropores (Figure 2c, inserted). The pore volume of POF-HS is also higher than that of POF-SS, being 0.775 and

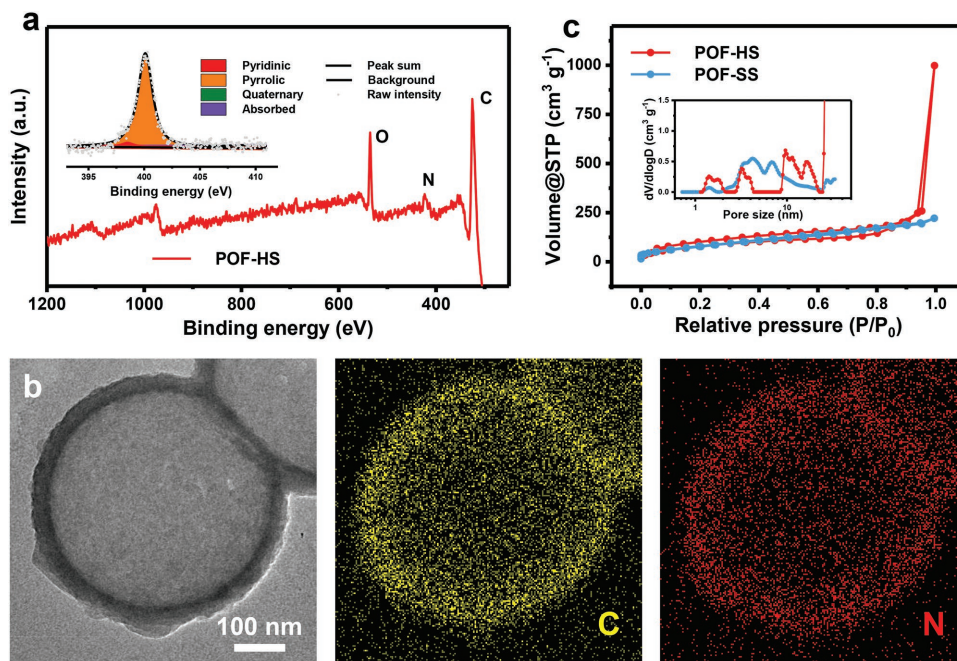


Figure 2. Characterization of POF-HS. a) XPS survey and inserted high-resolution N 1s XPS spectrum of POF-HS. b) TEM image and corresponding EDS mapping of POF-HS. c) N_2 sorption isotherms and inserted pore size distribution of POF-HS and POF-SS.

$0.303 \text{ cm}^3 \text{ g}^{-1}$, respectively. These features are attributed to the superior hollow interior of POF-HS over POF-SS.

The successful fabrication of hollow spherical POF encourages further morphology regulation to demonstrate the controllability and versatility of this synthetic strategy. Herein, the void size and the shell thickness are selected as two key parameters for morphology regulation, which are adjusted by simply altering relevant synthetic conditions. The void size is regulated by changing the size of PS templates. Using a PS template with a diameter of $0.10 \mu\text{m}$, small POF-HS (named as s-POF-HS) was fabricated (Figure S8a, Supporting Information). TEM images of s-POF-HS exhibit an inner diameter of $\approx 100 \text{ nm}$ in extremely good accordance with the size of the PS templates (Figure 3a and Figure S8b, Supporting Information). The shell thickness is 20 nm (Figure S8c, Supporting Information) and the N content of is $11.1 \text{ at.}\%$, similar to that of POF-HS (Figure S8d, Supporting Information). A larger PS template with the diameter of $4.5 \mu\text{m}$ was also applied (Figure S9a, Supporting Information), resulting in large POF-HS (named as l-POF-HS, Figure S3c) with a robust structure and a diameter of $\approx 4.7 \mu\text{m}$. The edge is intact without collapse (Figure S9b, Supporting Information) and the shell thickness is 80 nm (Figure S9c, Supporting Information). Taking account of the original POF-HS (Figure 3b), size regulation is proved to be highly effective with the hollow interior exactly duplicated from various PS templates.

Shell thickness regulation was performed by changing the mass ratio of POF substrates to PS templates. With less substrates added but the same PS templates as in the case of POF-HS synthesis, flimsy POF-HS (named as f-POF-HS) was fabricated. The diameter of f-POF-HS was unchanged (Figure 3d, inserted, and Figure S10a, Supporting Information). However, the shell thickness is prominently decreased to 20 nm (Figure 3d). The spherical morphology is partially deformed because of

the thin shell (Figure S10b, Supporting Information), but the hollow spheres are unbroken with intact edges (Figure S10c, Supporting Information). Thick-shell POF-HS (named as t-POF-HS) was synthesized with more POF precursors. The shell thickness increases to 60 nm and the diameter maintains as 500 nm , which is in agreement with the size of PS templates (Figure 3f and Figure S11a, Supporting Information). Thicker shell of POF-HS renders perfect replication of spherical morphology and layer stacking of POF building blocks (Figure S11b,c, Supporting Information). The above series of POF-HSs with varied shell thicknesses further indicate that the morphology of POF can be rationally regulated using modified synthetic routines to afford diversiform POF-HSs for energy storage applications.

Considering the conjugated porphyrin units with polar chemical structures and the unique hollow spherical morphology, POF-HS was applied in Li-S batteries as the host material of S cathodes. Li-S batteries feature high specific energy of 2600 Wh kg^{-1} , natural abundance, low cost, and nontoxicity of sulfur, making Li-S batteries as promising next-generation energy storage devices.^[30] However, challenges of S cathodes strongly postpone the practical applications of Li-S batteries. The dissolution of polysulfide intermediates as well as their poor interaction with typical nonpolar hosts such as carbon render notorious shuttling of polysulfides and great volume change through phase migration.^[31] Therefore, the capacity of practical Li-S batteries dramatically decays during cycling, along with other issues such as reduced Columbic efficiency (CE) and poor rate performance.

Rational design and selection of the host material is significant for constructing effective S cathodes with suppressed shuttle effect and alleviative volumetric change. Hollow spherical materials with polar chemical structures are highly considered as favorable host materials due to dual confinement

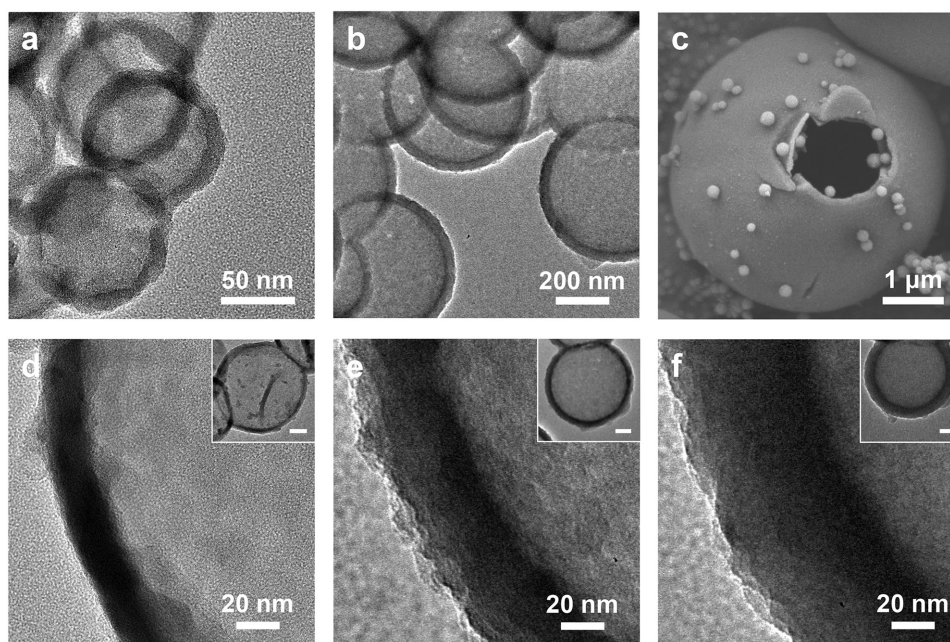


Figure 3. Morphology characterization of POF-HSs varying in void size and shell thickness. TEM images of a) s-POF-HS and b) POF-HS. c) Scanning electron microscope (SEM) image of l-POF-HS. TEM images of d) f-POF-HS, e) POF-HS, and f) t-POF-HS, respectively. Scale bars in the inserted TEM images are 100 nm.

effects.^[32] On one hand, polar functional groups possess sufficiently strong binding capability to anchor polar polysulfides through intermolecular chemical interactions.^[33] The adsorbed polysulfides are therefore immobilized at the cathode and the shuttling is suppressed. Nitrogen-doped carbon,^[34] inorganic additives,^[35] and polar polymers^[36] constitute typical examples according to the principle. On the other hand, the inner space of hollow spheres accommodates sulfur and tolerates the volumetric changes during cycling.^[37] Simultaneously, the hollow structure sterically retards the outward leakage of polysulfides.^[38] The two combined features contribute to synergistic dual confinements to polysulfides, benefiting the suppression of shuttle effect and high utilization of sulfur.

POF-HS with polar chemical structures and hollow spherical morphology therefore fully satisfies the above requirements for superior S hosts. Visualized adsorption of polysulfides was carried out to evaluate the adsorption of polysulfides by various host materials. Carbon black (CB) serves as the control sample with neither polar structures nor hollow morphology. As predicted, the solution of polysulfides quickly decolorized with POF-HS hosts but exhibited no change with regard to CB, implying the strong anchoring of polysulfides by POF-HS (Figure 4a). The abundant pore structures of POF-HS endow effective S diffusion and successful fabrication of the POF-HS/S cathode. The physical accommodation of sulfur within POF-HS was illustrated as neither discrete S nor structural collapse of POF-HS was observed (Figure S12, Supporting Information), and element mapping unambiguously demonstrates the S content uniformly distributed in the same area as C and N (Figure S13, Supporting Information). These results corporately indicate the compatibility of POF-HS to accommodate sulfur and further suggest POF-HS as an efficient sulfur host for high-performance Li-S batteries.

The electrochemical redox features of POF-HS/S cathode were characterized using cyclic voltammetry. The redox peaks of 2.0 and 2.3 V during discharging and 2.3 and 2.4 V during charging indicate effective electrochemical reactions of active species within the POF-HS/S cathode (Figure S14, Supporting Information). The cycling performance was evaluated at the current density of 0.5 C (1.0 C = 1672 mA g⁻¹) and the S loading was 1.1 mg cm⁻² (Figure 4b). Galvanostatic discharge-charge profiles of the first cycle demonstrate two plateaus and a high initial capacity of 955 mAh g⁻¹ for the POF-HS/S cathode (Figure S15, Supporting Information). Despite close initial capacity, the POF-HS/S cathode exhibits superior stability over the CB/S cathode with higher capacity and CE after cycling. The POF-HS/S cathode maintained a capacity of 773 mAh g⁻¹ while the capacity of CB-based one quickly decayed to 477 mAh g⁻¹ after 200 cycles. In addition, the CE of the POF-HS/S cathode was stable and close to 100%, suggesting the effective suppression of polysulfide shuttling. On the contrary, the CB/S cathode only afforded a reduced CE of 95% at the 200th cycle because of the nonpolarity of CB and its poor interaction with polysulfides. Despite the similar resistance features before cycling, the cell with CB/S cathode exhibits much higher charge transfer resistance than that of the POF-HS/S cathode after cycling, indicating better stability of the POF-HS/S cathode (Figure S16, Supporting Information). To further prove the shuttle inhibition toward Li metal anodes, morphology characterization of the anodes was evaluated after cycling. The surface of Li metal anodes with the POF-HS/S cathode is smooth and uniform (Figure S17, Supporting Information). In contrast, significant corrosion of Li metal anodes was observed with abundant Li dendrites for the CB/S cathode, indicating the polysulfide shuttling is effectively suppressed with the POF-HS host from another aspect. The superior stability of POF-HS/S cathode is attributed to the unique polar

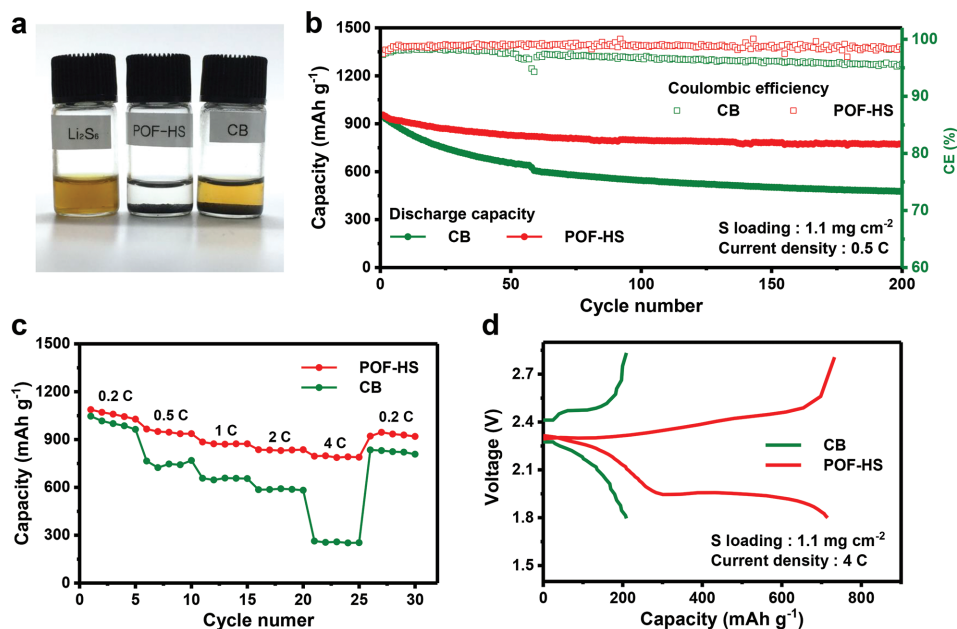


Figure 4. Electrochemical performance of POF-HS/S and CB/S cathodes. a) Visualized adsorption of polysulfides with POF-HS or CB after 24.0 h. b) Cycling performance at the current density of 0.5 C. c) Rate performance and d) corresponding galvanostatic discharge–charge profiles at 4.0 C. The sulfur loading is 1.1 mg cm⁻² for all the measurements.

structure and hollow morphology of POF-HS that provide favored microenvironments to immobilize polysulfides. The dual effects of chemical adsorption and physical accommodation promote the overall performance and confirm the superiority of POF-HS as the S host.

The rate performance of POF-HS- and CB-based S cathodes is characterized to evaluate the reaction kinetics of S. With the enhancement of current density, the capacity difference between POF-HS/S and CB/S cathodes becomes increasingly noteworthy (Figure 4c). Capacities of the POF-HS/S cathode remained stable at higher rates (870, 830, and 800 mAh g⁻¹ at 1.0, 2.0, and 4.0 C, respectively). In contrast, the CB/S cathode cannot sustain high-current-density operation and its capacities decayed to 650, 590, and 250 mAh g⁻¹ at 1.0, 2.0, and 4.0 C, respectively. Especially at 4.0 C, the POF-HS/S cathode still performed two extinct discharge plateaus, which unfortunately cannot be observed for the CB/S cathode (Figure 4d). Again, the POF-HS contributes to suppressing shuttling, propelling S reactions, relieving volumetric change, and ultimately improving the all-around performance of Li–S batteries.

In summary, hollow spherical porphyrin organic frameworks were fabricated following a template method. POF-HS exhibits explicit framework structures of 2D POF layers and controllable morphology of hollow spheres with varied void size and shell thickness. POF-HS functions as a desirable host material for S cathode in Li–S batteries, rendering high capacity, long-term stability, and excellent rate performance. The dual effects of chemical adsorption and physical accommodation of polysulfides, which are derived from the intrinsic polar nature and topological hollow structure of POF-HS, account for the enhancement in electrochemical performance of as-modified Li–S batteries. The accurate synthesis of the series of POF-HSs demonstrates the highly controllable and versatile morphology

of organic framework materials beyond chemical integration of organic building blocks and represents infinite feasibility of creating organic framework materials with precise nanostructures toward sustainable chemistry and material science.

Supporting Information

Supporting Information is available from the Wiley Online Library or from the author.

Acknowledgements

B.-Q.L., S.-Y.Z., and L.K. contributed equally to this work. This work was supported by National Key Research and Development Program (Nos. 2016YFA0202500 and 2016YFA0200102), National Natural Scientific Foundation of China (No. 21676160), and Tsinghua University Initiative Scientific Research Program. The authors thank Cheng Tang, Jin Xie, and Prof. Jia-Qi Huang for helpful discussion.

Conflict of Interest

The authors declare no conflict of interest.

Keywords

hollow spheres, lithium–sulfur batteries, porphyrin organic frameworks, precise synthesis, sulfur hosts

Received: December 22, 2017

Revised: March 13, 2018

Published online:

- [1] C. S. Diercks, O. M. Yaghi, *Science* **2017**, 355, 923.
- [2] N. Huang, P. Wang, D. L. Jiang, *Nat. Rev. Mater.* **2016**, 1, 16068.
- [3] A. P. Cote, A. I. Benin, N. W. Ockwig, M. O'Keeffe, A. J. Matzger, O. M. Yaghi, *Science* **2005**, 310, 1166.
- [4] S. Lin, C. S. Diercks, Y. B. Zhang, N. Kornienko, E. M. Nichols, Y. B. Zhao, A. R. Paris, D. Kim, P. Yang, O. M. Yaghi, C. J. Chang, *Science* **2015**, 349, 1208.
- [5] Y.-B. Zhang, J. Su, H. Furukawa, Y. Yun, F. Gandara, A. Duong, X. Zou, O. M. Yaghi, *J. Am. Chem. Soc.* **2013**, 135, 16336.
- [6] S. Wan, J. Guo, J. Kim, H. Ihee, D. Jiang, *Angew. Chem., Int. Ed.* **2008**, 47, 8826.
- [7] S. Kandambeth, B. P. Biswal, H. D. Chaudhari, K. C. Rout, S. H. Kunjattu, S. Mitra, S. Karak, A. Das, R. Mukherjee, U. K. Kharul, R. Banerjee, *Adv. Mater.* **2017**, 29, 1603945.
- [8] V. S. Vyas, F. Haase, L. Stegbauer, G. Savasci, F. Podjaski, C. Ochsenfeld, B. V. Lotsch, *Nat. Commun.* **2015**, 6, 8508.
- [9] B. J. Smith, W. R. Dichtel, *J. Am. Chem. Soc.* **2014**, 136, 8783.
- [10] S. Chandra, S. Kandambeth, B. P. Biswal, B. Lukose, S. M. Kunjir, M. Chaudhary, R. Babarao, T. Heine, R. Banerjee, *J. Am. Chem. Soc.* **2013**, 135, 17853.
- [11] W. Huang, Y. Jiang, X. Li, X. Li, J. Wang, Q. Wu, X. Liu, *ACS Appl. Mater. Interfaces* **2013**, 5, 8845.
- [12] S. Wan, J. Guo, J. Kim, H. Ihee, D. Jiang, *Angew. Chem., Int. Ed.* **2009**, 48, 5439.
- [13] a) X. Wang, J. Feng, Y. Bai, Q. Zhang, Y. Yin, *Chem. Rev.* **2016**, 116, 10983; b) L. Yu, H. Hu, H. B. Wu, X. W. Lou, *Adv. Mater.* **2017**, 29, 1604563.
- [14] N. Jayaprakash, J. Shen, S. S. Moganty, A. Corona, L. A. Archer, *Angew. Chem., Int. Ed.* **2011**, 50, 5904.
- [15] M.-Q. Zhao, X. Xie, C. E. Ren, T. Makaryan, B. Anasori, G. Wang, Y. Gogotsi, *Adv. Mater.* **2017**, 29, 1702410.
- [16] K. Fan, Y. Ji, H. Zou, J. Zhang, B. Zhu, H. Chen, Q. Daniel, Y. Luo, J. Yu, L. Sun, *Angew. Chem., Int. Ed.* **2017**, 56, 3289.
- [17] a) F. Xie, L. Zhang, D. Su, M. Jaroniec, S.-Z. Qiao, *Adv. Mater.* **2017**, 29, 1700989; b) H. Hu, B. Y. Guan, X. W. Lou, *Chemistry* **2016**, 1, 102.
- [18] J. Jiang, M. Gao, W. Sheng, Y. Yan, *Angew. Chem., Int. Ed.* **2016**, 55, 15240.
- [19] J. Shin, R. M. Anisur, M. K. Ko, G. H. Im, J. H. Lee, I. S. Lee, *Angew. Chem., Int. Ed.* **2009**, 48, 321.
- [20] T.-Y. Zhou, F. Lin, Z.-T. Li, X. Zhao, *Macromolecules.* **2013**, 46, 7745.
- [21] S. Kandambeth, V. Venkatesh, D. B. Shinde, S. Kumari, A. Halder, S. Verma, R. Banerjee, *Nat. Commun.* **2015**, 6, 6786.
- [22] A. Halder, S. Kandambeth, B. P. Biswal, G. Kaur, N. C. Roy, M. Addicoat, J. K. Salunke, S. Banerjee, K. Vanka, T. Heine, S. Verma, R. Banerjee, *Angew. Chem., Int. Ed.* **2016**, 55, 7806.
- [23] Y. Liu, J. Goebel, Y. Yin, *Chem. Soc. Rev.* **2013**, 42, 2610.
- [24] N. Kang, J. H. Park, M. Jin, N. Park, S. M. Lee, H. J. Kim, J. M. Kim, S. U. Son, *J. Am. Chem. Soc.* **2013**, 135, 19115.
- [25] B. Wang, J. S. Chen, H. B. Wu, Z. Wang, X. W. Lou, *J. Am. Chem. Soc.* **2011**, 133, 17146.
- [26] a) J. Tan, S. Namuangruk, W. Kong, N. Kungwan, J. Guo, C. Wang, *Angew. Chem., Int. Ed.* **2016**, 55, 13979; b) B. Sun, D. Wang, L. Wan, *Sci. China Chem.* **2017**, 60, 1098.
- [27] G. Zheng, S. W. Lee, Z. Liang, H.-W. Lee, K. Yan, H. Yao, H. Wang, W. Li, S. Chu, Y. Cui, *Nat. Nanotechnol.* **2014**, 9, 618.
- [28] a) L. J. Boucher, J. J. Katz, *J. Am. Chem. Soc.* **1967**, 89, 1340; b) D. W. Thomas, A. E. Martell, *J. Am. Chem. Soc.* **1959**, 81, 5111.
- [29] a) C. Tang, H.-F. Wang, X. Chen, B.-Q. Li, T.-Z. Hou, B. Zhang, Q. Zhang, M. M. Titirici, F. Wei, *Adv. Mater.* **2016**, 28, 6845; b) D. H. Guo, R. Shibuya, C. Akiba, S. Saji, T. Kondo, J. Nakamura, *Science* **2016**, 351, 361.
- [30] a) R. Fang, S. Zhao, Z. Sun, D. W. Wang, H. M. Cheng, F. Li, *Adv. Mater.* **2017**, 29, 1606823; b) J. Liang, Z.-H. Sun, F. Li, H.-M. Cheng, *Energy Storage Mater.* **2016**, 2, 76; c) H.-J. Peng, J.-Q. Huang, Q. Zhang, *Chem. Soc. Rev.* **2017**, 46, 5237; d) J. L. Wang, Y. S. He, J. Yang, *Adv. Mater.* **2015**, 27, 569.
- [31] a) A. Manthiram, S.-H. Chung, C. Zu, *Adv. Mater.* **2015**, 27, 1980; b) X. Tao, J. Wang, C. Liu, H. Wang, H. Yao, G. Zheng, Z. W. Seh, Q. Cai, W. Li, G. Zhou, C. Zu, Y. Cui, *Nat. Commun.* **2016**, 7, 11203; c) C. Ye, L. Zhang, C. Guo, D. Li, A. Vasileff, H. H. Wang, S. Z. Qiao, *Adv. Funct. Mater.* **2017**, 27, 1702524; d) M. Li, Y. N. Zhang, X. L. Wang, W. Ahn, G. P. Jiang, K. Feng, G. Liu, Z. W. Chen, *Adv. Funct. Mater.* **2016**, 26, 8408.
- [32] a) F. Wu, Y. S. Ye, R. J. Chen, T. Zhao, J. Qian, X. X. Zhang, L. Li, Q. M. Huang, X. D. Bai, Y. Cui, *Adv. Energy Mater.* **2017**, 7, 1601591; b) C. Zhang, H. B. Wu, C. Yuan, Z. Guo, X. W. Lou, *Angew. Chem., Int. Ed.* **2012**, 51, 9592; c) H.-J. Peng, J. Liang, L. Zhu, J.-Q. Huang, X.-B. Cheng, X. Guo, W. Ding, W. Zhu, Q. Zhang, *ACS Nano* **2014**, 8, 11280; d) G. M. Zhou, Y. B. Zhao, A. Manthiram, *Adv. Energy Mater.* **2015**, 5, 1402263; e) F. Boettger-Hiller, P. Kempe, G. Cox, A. Panchenko, N. Janssen, A. Petzold, T. Thurn-Albrecht, L. Borcharde, M. Rose, S. Kaskel, C. Georgi, H. Lang, S. Spange, *Angew. Chem., Int. Ed.* **2013**, 52, 6088; f) J. Zhang, C. P. Yang, Y. X. Yin, L. J. Wan, Y. G. Guo, *Adv. Mater.* **2016**, 28, 9539.
- [33] a) K. Mi, S. W. Chen, B. J. Xi, S. S. Kai, Y. Jiang, J. K. Feng, Y. T. Qian, S. L. Xiong, *Adv. Funct. Mater.* **2017**, 27, 1604265; b) T.-Z. Hou, W.-T. Xu, X. Chen, H.-J. Peng, J.-Q. Huang, Q. Zhang, *Angew. Chem., Int. Ed.* **2017**, 56, 8178; c) J. X. Song, M. L. Gordin, T. Xu, S. R. Chen, Z. X. Yu, H. Sohn, J. Lu, Y. Ren, Y. H. Duan, D. H. Wang, *Angew. Chem., Int. Ed.* **2015**, 54, 4325; d) T. Zhao, Y. S. Ye, C. Y. Lao, G. Divitini, P. R. Coxon, X. Y. Peng, X. He, H. K. Kim, K. Xi, C. Ducati, R. J. Chen, Y. J. Liu, S. Ramakrishna, R. V. Kumar, *Small* **2017**, 13, 1700357; e) J. Xu, T. Lawson, H. Fan, D. Su, G. Wang, *Adv. Energy Mater.* **2018**, 8, 1702607; f) D. Su, M. Cortie, H. Fan, G. Wang, *Adv. Mater.* **2017**, 29, 1700587.
- [34] F. Pei, T. An, J. Zang, X. Zhao, X. Fang, M. Zheng, Q. Dong, N. Zheng, *Adv. Energy Mater.* **2016**, 6, 1502539.
- [35] a) H.-J. Peng, Z.-W. Zhang, J.-Q. Huang, G. Zhang, J. Xie, W.-T. Xu, J.-L. Shi, X. Chen, X.-B. Cheng, Q. Zhang, *Adv. Mater.* **2016**, 28, 9551; b) W. Bao, D. Su, W. Zhang, X. Guo, G. Wang, *Adv. Funct. Mater.* **2016**, 26, 8746.
- [36] C.-Y. Chen, H.-J. Peng, T.-Z. Hou, P.-Y. Zhai, B.-Q. Li, C. Tang, W. Zhu, J.-Q. Huang, Q. Zhang, *Adv. Mater.* **2017**, 29, 1606802.
- [37] W. Li, G. Zheng, Y. Yang, Z. W. Seh, N. Liu, Y. Cui, *Proc. Natl. Acad. Sci. USA* **2013**, 110, 7148.
- [38] a) Z. Li, J. Zhang, B. Guan, D. Wang, L.-M. Liu, X. W. Lou, *Nat. Commun.* **2016**, 7, 13065; b) S. Chen, X. Huang, H. Liu, B. Sun, W. Yeoh, K. Li, J. Zhang, G. Wang, *Adv. Energy Mater.* **2014**, 4, 1301761.